Thermal Analysis of a Reactive Magnetohydrodynamic Flow through a Circular Cylindrical Pipe with Variable Fluid Properties

Anthony R. Hassan,[1] Hammed A. Ogunseye[2] and Olugbenga J. Fenuga[2]*

[1]Department of Mathematics, Tai Solarin University of Education, Ogun State, Nigeria
[2]Department of Mathematics, University of Lagos, Akoka-Yaba, Lagos, Nigeria

*ofenuga@unilag.edu.ng

_____

Abstract
This work considers the thermal analysis of an incompressible third-grade magnetohydrodynamic (MHD) steady fluid flow in a pipe with variable fluid properties; together with convective cooling at the walls. The momentum and energy equations regulating the flow are solved numerically by using the Runge–Kutta integration algorithm, combined with shooting technique. The solutions obtained are used to determine the numerical procedures for bifurcation analysis, skin-friction, heat transfer rate and thermal stability to predict the safe and unsafe situations of hazard prevention.

Keywords: convective cooling, cylindrical pipe, thermal criticality, Runge–Kutta integration

_____

Introduction

The investigation of thermal analysis of a third-grade fluid flow through a circular cylindrical pipe with variable fluid properties and convective cooling at the walls under the influence of magnetic field strength has abundant industrial and engineering applications as shown by Fosdick and Rajagopal (1980), Makinde (2014), Adesanya and Falade (2015), and Kobo and Makinde (2010).

Researchers have recently extended investigations to third-grade reactive fluids for their significance and roles in the production of hydrocarbon oils, grease, etc. Meanwhile, variable fluid properties such as viscosity and thermal conductivity, which describe the rate at which fluids conduct electricity and heat transfer with temperature gradients, are of high importance to enhance productivity in industries. However, as reported by Elgazery (2012), the appreciable relevance of hydromagnetic fluids exists in the refining of molten metals and non-metallic inclusions by the introduction of an electrically conducting fluid subject to magnetic field strengths that experience a force that results in current generation in the magnetohydrodynamic (MHD) fluid with applications in industrial and engineering processes. This improvement is needed in new technological trends to develop an appropriate mathematical model to understand fluid behaviour.

Other researchers like Makinde (2012, 2014), Makinde and Aziz (2010), Ajadi (2009), Ahmad (2009), Yurusoy *et al.* (2008), Hayat *et al.* (2008) and Mahmoud (2009) have extensively examined the flow of third-grade fluids with different properties and characteristics to determine the thermophysical properties, such as thermal stability, to predict the safe and unsafe situations of hazard prevention, the rate of disturbance with the second law of thermodynamics and variable fluid properties.

However, a considerable number of researchers mentioned above, have considered the properties of fluids to be constant but some of these properties can change with temperature especially when strong magnetic field strength is introduced as described by Elgazery (2012), Hayat *et al.* (2008), Mahmoud (2009), Ellahi and Riaz (2010), where efforts were made to critically examine the impact of magnetic field on the inner third-grade fluid flow through a pipe and especially in Ellahi and Riaz (2010) where viscosity depended upon the space coordinate.

This paper extends the work of Chinyoka and Makinde (2010) by examining the effects of magnetic field strength and variable fluid properties like thermal conductivity and fluid viscosity on a reactive MHD flow through a circular cylindrical pipe with convective cooling at the walls. The governing equations are solved numerically using the Runge–Kutta integration algorithm with shooting technique and implemented using a freely downloaded mathematical software (Maple software).

Materials and Methods

An incompressible, MHD steady flow of a third-grade fluid in a circular cylindrical pipe with convective cooling at the walls was considered. The geometry of the problem is shown in Figure 1. The

fluid is electrically conducting under the influence of a transversely applied magnetic field B_0. Employing the cylindrical coordinates $(\bar{r}, \varphi, \bar{z})$ with the $\bar{z}$-axis coinciding with the axis of the pipe, such that $\bar{r} = a$ is the radius of the pipe and φ is the azimuthal angle. Neglecting induced magnetic field and chemical reactions, the linear velocity and energy equations describing the fluid flow in non-dimensionless form are as expressed by Chinyoka and Makinde (2010), Makinde (2012) and Okoya (2016).
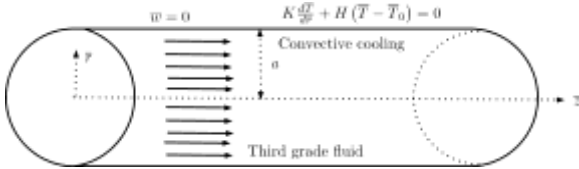

Figure 1: Geometry of the problem

$$\frac{1}{\bar{r}} \frac{d}{d\bar{r}}\left(\bar{r}\bar{\mu}(T)\frac{d\bar{\omega}}{d\bar{r}}\right) + \frac{2\bar{\beta}_3}{\bar{r}}\frac{d}{d\bar{r}}\left(\bar{r}\left(\frac{d\bar{\omega}}{d\bar{r}}\right)^2\right) - \sigma\bar{\beta}_0^2\bar{\omega} - \frac{\partial\bar{p}}{d\bar{z}} = 0,$$

(1)

$$\frac{1}{\bar{r}} \frac{d}{d\bar{r}}\left(\bar{r}K(\bar{T})\frac{d\bar{T}}{d\bar{r}}\right) + \left(\frac{d\bar{\omega}}{d\bar{r}}\right)^2\left(\bar{\mu}(\bar{T}) + 2\bar{\beta}_3\left(\frac{d\bar{\omega}}{d\bar{r}}\right)^2\right)$$

(2)

$$+ QC_0A_0 \exp\left(-\frac{E}{RT}\right) + \sigma\bar{\beta}_0^2\bar{\omega}^2 = 0.$$

The flow is symmetric about the z-axis; there is heat exchange at the pipe surface with the ambient temperature following Newton's cooling law and then the appropriate boundary conditions are

$$\frac{d\bar{\varpi}}{d\bar{r}} = \frac{d\bar{T}}{d\bar{r}} = 0 \qquad at \qquad \bar{r} = 0$$

(3)

$$\bar{\omega} = 0, \quad K(\bar{T})\frac{d\bar{T}}{d\bar{r}} = -H(\bar{T} - \bar{T}_0) \; at \quad \bar{r} = a$$

(4)

where $\bar{r}$ is the radial distance measured in the normal direction $\bar{\mu}$, is the temperature dependent viscosity, $\bar{\omega}$ is the dimensional axial velocity, β_3 is the material coefficient, σ represents electrical conductivity, $(\partial\bar{p})/(d\bar{z})$ the emerging pressure gradients in the axial direction, $\bar{p}$ is the dimensional modified pressure $\bar{T}$, is the absolute temperature, $K(\bar{T})$ is the temperature dependent thermal conductivity, Q is the heat of reaction C_0, is the initial concentration of the reactant species, A_0 is the rate constant, E is the activation energy, R is the universal gas constant, $\bar{T}_0$ is the absolute temperature of the surrounding environment, H is the surface heat transfer coefficient and a is the pipe radius.

The Arrhenius model is usually used to describe the variations of viscosity with temperature in a variety of fluid and mass flows because it is well known that the viscosity of a liquid decreases with increasing temperature. The Arrhenius model for viscosity can be written as follows:

$$\bar{\mu}(\bar{T}) = \exp\left(\frac{E}{R\bar{T}}\right)$$

(5)

The temperature dependent thermal conductivity K of the fluid can be expressed in the form of Makinde (2009, 2012), Lacey and Wake (1982) as:

$$K(\bar{T}) = K_0 \exp\left[M(\bar{T} - \bar{T}_0)\right]$$

(6)

where K_0 is the material thermal conductivity at $\bar{T}_0$ and $M > 0$ is the thermal conductivity exponent variation parameter.

The following variables and parameters are introduced to non-dimensionalise equations (1)– (6):

$$r = \frac{\bar{r}}{a}, \qquad \omega = \frac{\bar{\omega}}{\omega_0}, \qquad \mu = \frac{\bar{\mu}}{\mu_0}, \qquad \Lambda = \frac{2\bar{\beta}_3\bar{\omega}_0^2}{\mu_0 a^2},$$

$$C = \frac{a^2}{\mu_0\omega_0}\frac{\partial\bar{p}}{\partial\bar{z}}, \quad \varepsilon = \frac{R\bar{T}_0}{E}, \quad \theta = \frac{E(\bar{T} - \bar{T}_0)}{R\bar{T}_0^2},$$

$$Ha^2 = \frac{\sigma B_0^2 a^2}{\mu_0}, \quad n = M\varepsilon\bar{T}_0, \quad \Gamma = \frac{\bar{\omega}_0^2\mu_0}{k_0\bar{T}_0\varepsilon}, \quad Bi = \frac{Ha}{K_0}$$

$$B_i = \frac{H_a}{K_0} = \sqrt{\frac{\sigma}{\mu_0}}B_0 a$$

and $\delta = \frac{QEA_0 a^2 C_0}{\bar{T}^2 RK_0}\exp\left(-\frac{E}{R\bar{T}_0}\right)$

(7)

where ω_0 is a reference velocity. Here r is the dimensionless perpendicular distance from the pipe axis, ω is the dimensionless velocity Γ is the viscous heating parameter, Ha is the Hartmann number, δ is the Frank–Kamenetskii parameter, θ is the dimensionless temperature excess, C is the pressure gradient parameter, Λ is the non-Newtonian material parameter of the fluid, ε is the activation energy parameter, B_i is the Biot number, n is the parameter representing the ratio of temperature-dependent thermal conductivity to heat production, μ_0 is the material variation of viscosity at $\bar{T}_0$ and k_0 is the material thermal conductivity at $\bar{T}_0$. Using the above non-dimensional variables and parameters (7), equations (1)– (6) take the form:

$$\frac{1}{r}\frac{d}{dr}\left(r\mu(\theta)\frac{d\varpi}{dr}\right) + \frac{\Lambda}{r}\frac{d}{dr}\left(r\left(\frac{d\varpi}{dr}\right)^3\right) - Ha^2\varpi - C = 0.$$

(8)

$$\frac{1}{r}\frac{d}{dr}\left(r\frac{d\theta}{dr}\right)+n\left(r\frac{d\theta}{dr}\right)^3+\exp(-n\theta)\Gamma\left[\left(\frac{d\varpi}{dr}\right)^2\left(\mu(\theta)+\Lambda\left(\frac{d\varpi}{dr}\right)^2\right)+Ha^2\omega^2\right]$$

$$+\delta\exp\left(\frac{\theta}{1+\varepsilon\theta}\right)\exp(-n\theta)=0.$$

(9)

subject to the following boundary conditions

$$\frac{d\omega}{dr}=\frac{d\theta}{dr}=0,\quad at\quad r=0 \tag{10}$$

$$\omega=0,\ \frac{d\theta}{dr}=-Bi\theta\exp(-n\theta)\quad at\quad r=1 \tag{11}$$

The non-dimensionalised form of the temperature dependent viscosity is given by

$$\mu(\theta)=\exp\left(-\frac{\theta}{1+\varepsilon\theta}\right) \tag{12}$$

The physical quantities of interest are the skin-friction parameter C_f at the wall and the heat transfer rate at the wall, which is estimated in terms of Nusselt number (Nu) and are defined as follows:

$$C_f=d\omega/dr\big|_{r=1}=\omega'(1),\ \ Nu=d\theta/dr\big|_{r=1}=-\theta'(1) \tag{13}$$

The solutions to the governing equations (8) and (9), subject to the boundary conditions stated in equations (10) and (11), are solved using the Runge–Kutta method with shooting technique. Firstly, we observed that a singularity exists in equation (8) at $r=0$. This singularity was handled by evaluating equation (8) using the L'Hospital rule as described by Okoya (2016).

$$\lim_{r\to0}\left(\frac{1}{r}\frac{d\omega}{dr}\right)=\frac{d^2\omega}{dr^2} \tag{14}$$

Using equation (12), then equation (8) becomes

$$\frac{d}{dr}\left(\mu\frac{d\omega}{dr}\right)+2\mu\frac{d^2\omega}{dr^2}+6\Lambda\left(\frac{d\omega}{dr}\right)^2\frac{d^2\omega}{dr^2}-Ha^2\omega-C=0 \tag{15}$$

Putting equation (12) into (15), then (15) is simplified as

$$2\mu\frac{d^2\omega}{dr^2}-\frac{\mu}{(1+\varepsilon\theta)^2}\frac{d\theta}{dr}\frac{d\omega}{dr}+6\Lambda\left(\frac{d\omega}{dr}\right)^2\frac{d^2\omega}{dr^2}-Ha^2\omega-C=0 \tag{16}$$

The nonlinear differential equaotins (16) and (9) are then transformed into first-order differential equations as follows:

$$\begin{bmatrix}y_1\\y_2\\y_3\\y_4\end{bmatrix}'=\begin{bmatrix}y_2\\\dfrac{y_2y_4\exp\left(-\dfrac{y_3}{1+\varepsilon y_3}\right)+(1+\varepsilon y_3)^2(Ha^2y_1+C)}{(1+\varepsilon y_3)^2(6\Lambda y_2^2+2)}\\y_4\\-\dfrac{1}{2}y_4-ny_4^2-\Gamma\exp(-ny_3)\left(y_2^2\exp\left(-\dfrac{y_3}{1+\varepsilon y_3}\right)+\Lambda y_2^4+Ha^2y_2^2\right)-\delta\exp\left(\dfrac{y_3}{1+\varepsilon y_3}\right)\end{bmatrix} \tag{17}$$

Subject to the boundary conditions

$$y_1(0)=\alpha_1,\ y_2(0)=0,\ y_3(0)=\alpha_2,\ y_4(0)=0$$
$$y_1(1)=\alpha_1,\ y_4(1)=-Biy_3\exp(-ny_3) \tag{18}$$

where the prime denotes derivatives with respect to r and the undermined initial conditions α_i ($i=1,2$) are systematically assumed and evaluated iteratively. Then, equation (17) is solved numerically as an initial valued problem until the boundary condition at $r=1$ is satisfied. Convergence is attained for all given values of the parameters when the absolute value of the unknown, α_i ($i=1,2$) for previous computations differs by 10^{-8} at $r=1$.

Consider the one bifurcation parameter family of a two-point boundary-valued problem

$$y'=\vec{f}(t,\vec{y},\lambda),\ \vec{r}(\vec{y}(a),\vec{y}(b))=0 \tag{19}$$

Such that *a* and *b* are on the interval where the radius

of the circular cylinder lies and

$$\vec{y}(t)=\vec{y}(y_1(t),y_2(t),...y_n(t)),\ \vec{f}(t,\vec{y},\lambda)$$

is a vector function where the boundary conditions consist of *n* scalar equations.

$$\eta\big(y_1(a),\ldots,y_n(a),y_1(b),\ldots,y_n(b)\big)=0$$
$$\vdots \qquad\qquad =\vdots$$
$$r_n\big(y_1(a),\ldots,y_n(a),y_1(b),\ldots,y_n(b)\big)=0$$

(20)

where $\vec{y}'=\dfrac{d\vec{y}}{dt}$.

The linearisation of equation (19) with respect to *y* is the boundary-valued problem.

$$\left.\begin{array}{l}\vec{h}'=\vec{f}_y(t,\vec{y},\lambda)\vec{h}\\\vec{A}\vec{h}(a)+\vec{B}\vec{h}(b)=0\end{array}\right\} \tag{21}$$

where $\vec{h}(t)$ is a vector-valued function that consists

of n components, $\vec{f}_y = \dfrac{d\vec{f}}{d\vec{y}}$ is the Jacobian matrix,

$\vec{A}$ and $\vec{B}$ are the n^2 matrices of the linearisation of the boundary conditions,

$$\vec{A} = \frac{\partial \vec{r}(\vec{y}(a), \vec{y}(b))}{\partial \vec{y}(a)}, \quad \vec{B} = \frac{\partial \vec{r}(\vec{y}(a), \vec{y}(b))}{\partial \vec{y}(b)} \qquad (22)$$

Evaluated at bifurcation point $(\vec{y}_0, \lambda_0)$, the linearised problem in equation (21) has a nontrivial solution $\vec{h} \neq 0$. For $(\vec{y}, \lambda) \neq (\vec{y}_0, \lambda_0)$, the only solution to equation (21) is when $\vec{h} = 0$. We impose the equation $h_k(a) = 1$ on equation (21), where k are the numbers of unspecified initial conditions, these initial conditions enforce $\vec{h} \neq 0$. Hence, a bifurcation point is characterized by

$$\xi(\vec{y}, \lambda) = h_k(a) - 1 = 0 \qquad (23)$$

Equation (23) is for a solution $\vec{h}$ of equation (21), which depends on $(\vec{y}, \lambda)$. Following Seydel (1979, 2009) and Song *et al.* (1989), the branching system of differential equations regulating the fluid flow is given as:

$$\begin{pmatrix} \vec{y} \\ \lambda \\ \vec{h} \end{pmatrix}' = \begin{pmatrix} \vec{f}(t, \vec{y}, \lambda) \\ 0 \\ \vec{f}_y(t, \vec{y}, \lambda) \end{pmatrix}, \quad \begin{pmatrix} \vec{r}(\vec{y}(a), \vec{y}(b)) \\ h_k(a) - 1 \\ \vec{A}\vec{h}(a) + \vec{B}\vec{h}(b) \end{pmatrix} = 0 \qquad (24)$$

Equation (24) can then be solved by any standard ODE solver.

This section is used to calculate the branching behaviour of equations (8) and (24) with the boundary conditions (10) and (11). The bifurcation parameter in the equations is the Frank–Kamenettski parameter (δ). The values of $\theta_{\max cr}$ and $\delta_{\max cr}$ for varying various parameters are shown in Table 1.

Table 1: Effects of Various Parameters on Thermal Criticality values in Arrhenius Model

Λ	Ha	C	N	Γ	E	B_i	$\theta_{\max cr}$	$\delta_{\max cr}$
1	1	−1	0.05	1	0.1	5	1.88290254	1.57846568
2	1	−1	0.05	1	0.1	5	1.88017641	1.58436341
3	1	−1	0.05	1	0.1	5	1.87777144	1.58782094
1	1	−1	0.05	1	0.1	5	1.88290254	1.57846568
1	2	−1	0.05	1	0.1	5	1.87680838	1.58850989
1	3	−1	0.05	1	0.1	5	1.86619341	1.60051945
1	1	−3	0.05	1	0.1	5	2.14147997	1.40207243
1	1	−2	0.05	1	0.1	5	1.99502956	1.49623296
1	1	−1	0.05	1	0.1	5	1.88290254	1.57846568
1	1	−1	−0.05	1	0.1	5	1.73782786	1.45904985
1	1	−1	−0.01	1	0.1	5	1.79104276	1.50415420
1	1	−1	0	1	0.1	5	1.80526468	1.51595364
1	1	−1	0.01	1	0.1	5	1.81989150	1.52797663
1	1	−1	0.05	1	0.1	5	1.88290254	1.57846568
1	1	−1	0.05	1	0.1	5	1.88290254	1.57846568
1	1	−1	0.05	2	0.1	5	1.93004616	1.53499289
1	1	−1	0.05	3	0.1	5	1.97910380	1.49231838
1	1	−1	0.05	1	0	5	1.41936750	1.38025501
1	1	−1	0.05	1	0.01	5	1.45285499	1.39687258
1	1	−1	0.05	1	0.05	5	1.60961397	1.46956432
1	1	−1	0.05	1	0.1	5	1.88290254	1.57846568
1	1	−1	0.05	1	0.1	5	1.88290254	1.57846568
1	1	−1	0.05	1	0.1	10	1.89616971	1.89193806
1	1	−1	0.05	1	0.1	15	1.89820788	2.01725704
1	1	−1	0.05	1	0.1	1×10^2	1.89756548	2.25867856
1	1	−1	0.05	1	0.1	1×10^3	1.89690300	2.30059490
1	1	−1	0.05	1	0.1	1×10^4	1.89681983	2.30526873
1	1	−1	0.05	1	0.1	1×10^8	1.89681898	2.30531596

Results and Discussion

The data in Table 1 shows that increasing the values of the non-Newtonian parameter (Λ), magnetic field parameter (Ha), pressure gradient (C), the ratio of temperature-dependent thermal conductivity (n) and Biot number B_i decreases maximum velocity, maximum temperature and the Nusselt number.

However, increase in the Frank–Kamenettski parameter (δ) and viscous heating parameter (Γ) leads to corresponding increases in the Nusselt number, maximum velocity and maximum temperature. The skin friction rises with increasing values of non-Newtonian parameter (Λ), magnetic field parameter (Ha), pressure gradient (C) and Biot number B_i but

decreases with the Frank–Kamenettski parameter (δ), viscous heating parameter (Γ) and the ratio of temperature-dependent thermal conductivity (n).

Table 1 shows the effects of various parameters on the thermal criticality values in Arrhenius model. The $\theta_{max\,cr}$ reduces with the rising values of Newtonian parameter (Λ), magnetic field parameter (Ha) and pressure gradient (C) while $\theta_{max\,cr}$ rises with the rising values of the ratio of temperature-dependent

thermal conductivity (n), viscous heating parameter (Γ), activation energy parameter (ε) and Biot number B_i. Also, $\delta_{max\,cr}$ increases as all the thermophysical parameters increase but decreases with increase in the viscous heating parameter (Γ).

The computational results of the influence of the embedded thermophysical parameters on the maximum velocity ω_{max} and heat transferred θ_{max} with the skin-friction and Nusselt number are shown in Table 2.

Table 2: Effects of Various Parameters in Arrhenius Model

Λ	Ha	C	n	Γ	δ	B_i	ω_{max}	θ_{max}	C_f	Nu
1.0	1.0	−1.0	0.5	1.0	0.1	5.0	0.204115	0.063069	−0.395639	0.101599
3.0	1.0	−1.0	0.5	1.0	0.1	5.0	0.187599	0.060228	−0.341705	0.096315
5.0	1.0	−1.0	0.5	1.0	0.1	5.0	0.176991	0.058475	−0.311991	0.093107
1.0	1.0	−1.0	0.5	1.0	0.1	5.0	0.204115	0.063069	−0.395639	0.101599
1.0	2.0	−1.0	0.5	1.0	0.1	5.0	0.140245	0.060619	−0.323882	0.088163
1.0	3.0	−1.0	0.5	1.0	0.1	5.0	0.088815	0.054976	−0.258122	0.076575
1.0	1.0	−1.5	0.5	1.0	0.1	5.0	0.293626	0.093401	−0.539172	0.157325
1.0	1.0	−1.0	0.5	1.0	0.1	5.0	0.204115	0.063069	−0.395639	0.101599
1.0	1.0	−0.5	0.5	1.0	0.1	5.0	0.105610	0.042898	−0.216072	0.064320
1.0	1.0	−1.0	−1.0	1.0	0.1	5.0	0.204181	0.063998	−0.395634	0.102678
1.0	1.0	−1.0	0.0	1.0	0.1	5.0	0.204115	0.063069	−0.395639	0.101599
1.0	1.0	−1.0	0.5	1.0	0.1	5.0	0.203474	0.054921	−0.395348	0.093995
1.0	1.0	−1.0	0.5	1.0	0.1	5.0	0.204115	0.063069	−0.395639	0.101599
1.0	1.0	−1.0	0.5	2.0	0.1	5.0	0.207141	0.090999	−0.398029	0.152974
1.0	1.0	−1.0	0.5	3.0	0.1	5.0	0.210234	0.119476	−0.400468	0.205025
1.0	1.0	−1.0	0.5	1.0	0.01	5.0	0.200378	0.022889	−0.393223	0.048264
1.0	1.0	−1.0	0.5	1.0	0.05	5.0	0.201761	0.037287	−0.394156	0.068813
1.0	1.0	−1.0	0.5	1.0	0.1	5.0	0.203526	0.055605	−0.395344	0.094921
1.0	1.0	−1.0	0.5	1.0	0.1	3.0	0.205396	0.068904	−0.398528	0.095299
1.0	1.0	−1.0	0.5	1.0	0.1	5.0	0.203526	0.055605	−0.395344	0.094921
1.0	1.0	−1.0	0.5	1.0	0.1	10.0	0.202149	0.045812	−0.392990	0.094641

The present numerical scheme is validated by comparing the maximum velocity, ω_{max} and temperature maximum, θ_{max} with exiting numerical results available in the Literature as shown in Table 3. It can be seen that the computed values of ω_{max} and θ_{max} by the equations (17) and (18) are in perfect agreement with previous results.

Table 3: Values of $\omega_{max}(0)$ and $\theta_{max}(0)$ compared with Okoya (2016)

Λ	ω_{max}		θ_{max}	
	Ref	Present	Ref	Present
0	0.252650	0.252650	0.015811	0.015811
5	0.192455	0.192455	0.012149	0.012149
10	0.171515	0.171515	0.010810	0.010810
15	0.158764	0.158764	0.009989	0.009990

$\Gamma = -C = 1, Ha = n = \delta = \varepsilon = 0, B_i = 10^{-8}$

The graphical presentation showing the momentum and energy distributions for different values of the non-Newtonian parameter (Λ) are shown in Figures 2 and 3. The plots reveal that both fluid motion and

energy reduce as Λ increases. Figures 4 and 5 display the velocity and temperature profiles, respectively, for the variations in the value of the magnetic field strength (Ha). The increase in Ha retards the fluid motion and heat transfer due to the presence of Lorentz force across the flow channel.

The velocity and temperature profiles revealing the graphical representations of the impact of the ratio of temperature-dependent thermal conductivity (n) are shown in Figures 6 and 7, respectively. It can be seen that velocity and temperature decrease as thermal conductivity (n) increases from −1 to +1. This is due to the role of activation energy and wall temperature in the flow channel. The velocity and temperature distributions showing the impact of viscous heating (Γ) are shown in Figures 8 and 9, respectively. On a normal note, the fluid motion and temperature rise due to the viscous heating within the flow region. Moreover, there are increases in fluid motion and temperature as the Frank–Kamenettski parameter (δ) increases as displayed in Figures 10 and 11 due to the

compound effects of the initial concentrations of the reactant species, heat of reaction and the radius of the circular cylindrical pipe.

Finally, Figures 12 and 13 display the effects of the convective cooling parameter (B_i) on the velocity and temperature distributions. These Figures revealed that the fluid motion and temperature were reduced with the rising values of Bi; it mainly depends on the magnetic field strength and the thermal conductivity of the material medium.
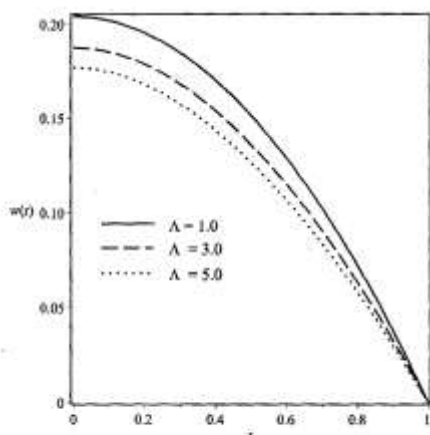

Figure 2: Velocity profile for various non-Newtonian parameter (Λ) when $Ha = -C = \Gamma = 1$, $n = 0.5$, $\delta = \varepsilon = 0.1$ and $Bi = 5$
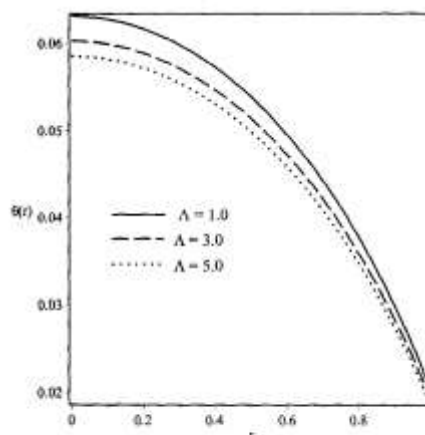
Figure 3: Temperature Profiles for various non-Newtonian parameter (Λ) when $Ha = -C = \Gamma = 1$, $n = 0.5$, $\delta = \varepsilon = 0.1$ and $Bi = 5$
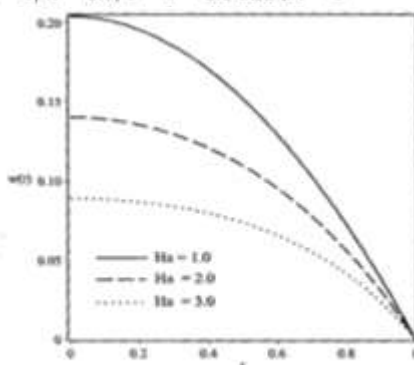
Figure 4: Velocity profile for various magnetic field intensity (Ha) when $\Lambda = -C = \Gamma = 1$, $n = 0.5$, $\delta = \varepsilon = 0.1$ and $Bi = 5$
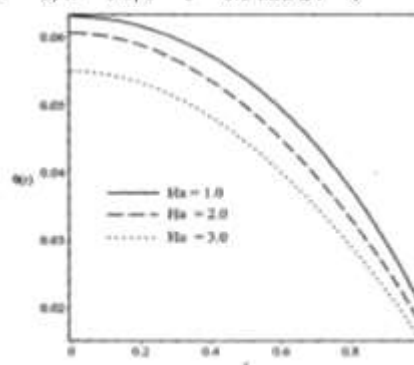
Figure 5: Temperature Profile for various magnetic field intensity (Ha) when $\Lambda = -C = \Gamma = 1$, $n = 0.5$, $\delta = \varepsilon = 0.1$ and $Bi = 5$
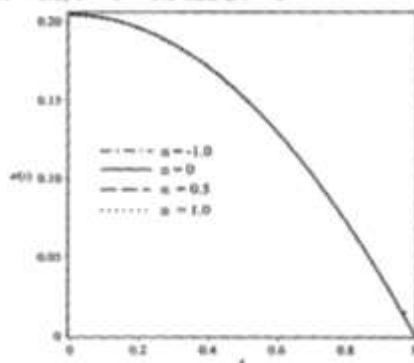

Figure 6: Velocity profile for various ratio of temperature-dependent thermal conductivity (n) when $\Lambda = Ha = -C = \Gamma = 1$, $\delta = \varepsilon = 0.1$ and $Bi = 5$
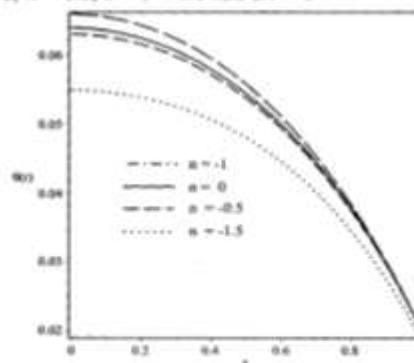

Figure 7: Temperature Profiles for various ratio of temperature-dependent thermal conductivity (n) when $\Lambda = Ha = -C = \Gamma = 1$, $n = 0.5$, $\delta = \varepsilon = 0.1$ and $Bi = 5$
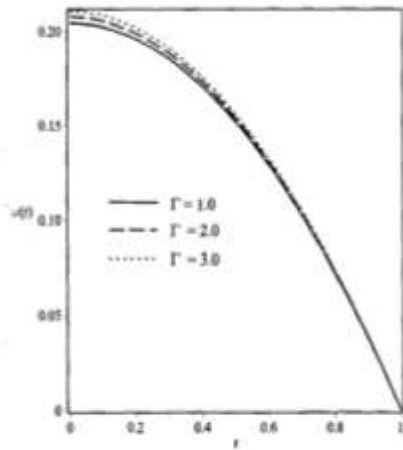
Figure 8: Velocity profile for various viscous heating parameter (Γ) when $\Lambda = Ha = -C = 1$, $\delta = \varepsilon = 0.1$, $n = 0.5$ and $Bi = 5$
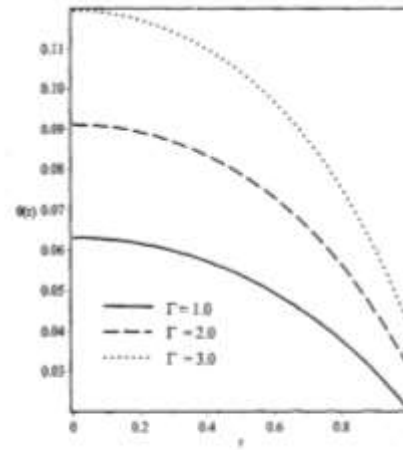

Figure 9: Temperature Profiles for various viscous heating parameter (Γ) when $\Lambda = Ha = -C = 1$, $n = 0.5$, $\delta = \varepsilon = 0.1$, $n = 0.5$ and $Bi = 5$
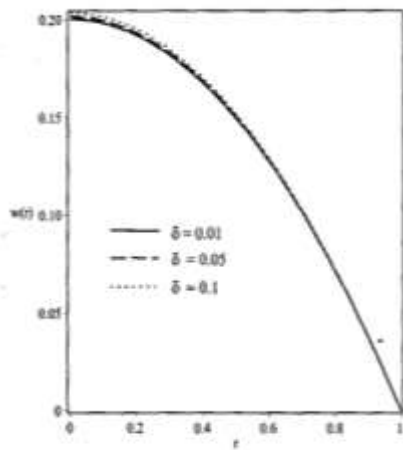

Figure 10: Velocity profile for various Frank-Kamenetskii parameter (δ) when $\Lambda = \Gamma = Ha = -C = 1$, $\varepsilon = 0.1$, $n = 0.5$ and $Bi = 5$
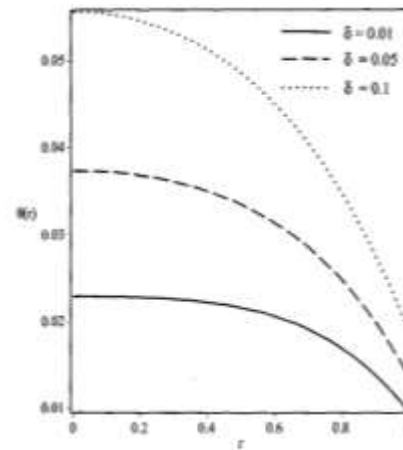

Figure 11: Temperature Profiles for various Frank-Kamenetskii parameter (δ) when $\Lambda = \Gamma = Ha = -C = 1$, $n = 0.5$, $\varepsilon = 0.1$, $n = 0.5$ and $Bi = 5$
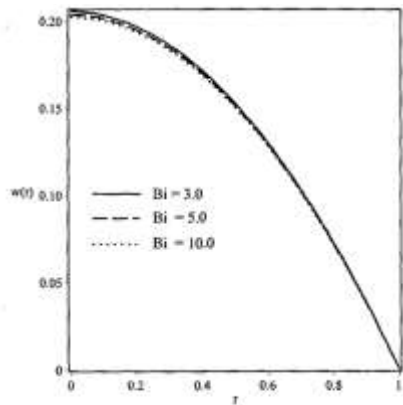

Figure 12: Velocity profile for various Biot number (Bi) when $\Lambda = \Gamma = Ha = -C = 1$, $\delta = \varepsilon = 0.1$ and $n = 0.5$
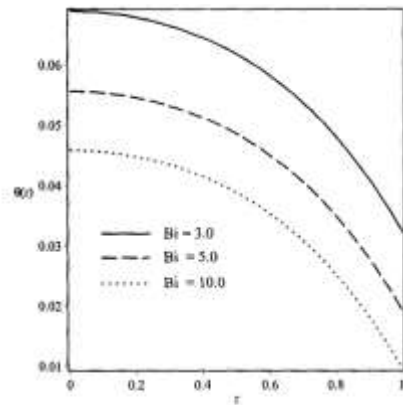

Figure 13: Temperature Profiles for various Biot number (Bi) when $\Lambda = \Gamma = Ha = -C = 1$, $\delta = \varepsilon = 0.1$ and $n = 0.5$

References

Adesanya, S. O. and Falade, J. A. (2015) Thermodynamics analysis of hydromagnetic third grade fluid flow through a channel filled with porous medium. *Alexandria Engineering Journal*, **54**(3)**:** 615–622.

Ahmad, F. (2009) A simple analytical solution for the steady flow of a third grade fluid in a porous half space. *Communications in Nonlinear Science and Numerical Simulation*, **14**(7): 2848–2852.

Ajadi, S. O. (2009) A note on the thermal stability of a reactive non-newtonian flow in a cylindrical pipe. *International Communications in Heat and Mass Transfer,* **36**(1): 63–68.

Chinyoka, T. and Makinde, O. D. (2010) Computational dynamics of unsteady flow of a variable viscosity reactive fluid in a porous pipe. *Mechanics Research Communications*, **37**(3): 347–353.

Elgazery, N. S. (2012) Effects of variable fluid properties on natural convection of MHD fluid from a heated vertical wavy surface. *Meccanica*, **47**(5): 1229–1245.

Ellahi, R. and Riaz, A. (2010) Analytical solutions for MHD flow in a third-grade fluid with variable viscosity. *Mathematical and Computer Modeling*, **52**(9): 1783–1793.

Fosdick, R. L. and Rajagopal, K. R. (1980) Thermodynamics and stability of fluids of third grade. *Proceedings of the Royal Society of London A: Mathematical, Physical and Engineering Sciences 369***,** p. 351–377.

Hayat T., Ahmed N. and Sajid M. (2008) Analytic solution for MHD flow of a third order fluid in a porous channel. *Journal of Computational and Applied Mathematics*, **214**(2): 572–582.

Kobo, N. S. and Makinde, O. D. (2010) Second law analysis for a variable viscosity reactive Couette flow under Arrhenius kinetics. *Mathematical Problems in Engineering*, **2010:** 1–15.

Lacey, A. A. and Wake, G. C. (1982) Thermal ignition with variable thermal conductivity. *IMA Journal of Applied Mathematics*, **28**(1): 23–39.

Mahmoud, M. A. A. (2009) Thermal radiation effect on unsteady MHD free convection flow past a vertical plate with temperature-dependent viscosity. *The Canadian journal of chemical engineering,* **87**(1): 47–52.

Makinde, O. D. (2008) Entropy-generation analysis for variable-viscosity channel flow with non-uniform wall temperature. *Applied Energy*, **85**(5): 384–393.

Makinde, O. D. (2009) Thermal stability of a reactive viscous flow through a porous-saturated channel with convective boundary conditions. *Applied Thermal Engineering*, **29**(8): 1773–1777.

Makinde, O. D. (2012) On the thermal decomposition of reactive materials of variable thermal conductivity and heat loss characteristics in a long pipe. *Journal of Energetic Materials*, **30**(4): 283–298.

Makinde, O. D. (2014) Thermal analysis of a reactive generalized couette flow of power law fluids between concentric cylindrical pipes. *The European Physical Journal Plus*, **129**(12): 1–9.

Makinde, O. D. and Aziz, A. (2010) Second law analysis for a variable viscosity plane Poiseuille flow with asymmetric convective cooling. *Computers and Mathematics with Applications*, **60**: 3012–3019.

Okoya, S. S. (2016) Flow, thermal criticality and transition of a reactive third-grade fluid in a pipe with Reynolds' model viscosity. *Journal of Hydrodynamics, Ser. B*, **28**(1): 84–94.

Seydel, R. (1979) Numerical computation of branch points in ordinary differential equations. *Numerische Mathematik,* **32**(1): 51–68.

Seydel, R. (2009) Practical bifurcation and stability analysis, Volume 5. Springer Science & Business Media, Netherland, p. 13–18.

Song X., Schmidt, L. D. and Aris, R. (1989) Shooting method for bifurcation analysis of boundary value problems. *Chemical Engineering Communications*, **84**(1): 217–229.

Yurusoy, M., Pakdemirli, M. and Yilbaş, B. S. (2008) Perturbation solution for a third-grade fluid flowing between parallel plates. *Proceedings of the Institution of Mechanical Engineers, Part C: Journal of Mechanical Engineering Science*, **222**(4): 653–656.